Experimental and Numerical Determination of Interface Slip Coefficient of Fluid Stream Exiting a Partially Filled Porous Medium Channel

Arunn Narasimhan[1]
Associate Professor
Department of Mechanical Engineering,
Indian Institute of Technology Madras,
Chennai 600 036, India
e-mail: arunn@iitm.ac.in

K. S. Raju
Department of Mechanical Engineering,
Indian Institute of Technology Madras,
Chennai 600 036, India

S. R. Chakravarthy
Professor
Department of Aerospace Engineering,
Indian Institute of Technology Madras,
Chennai 600 036, India

Stacks of parallel plates modeled as a standard fissure-type anisotropic porous medium are filled inside a rectangular channel up to half the cross section height. The interface slip coefficient α for the isothermal laminar incompressible flow exiting this partially filled porous-medium channel is then determined using particle image velocimetry (PIV) experiments and numerical simulations. Required measurements of the Darcy velocity u_D on the porous-medium (PM) side, the local velocity u_f, and its gradient $\partial u_f / \partial y$ on the clear-fluid (CF) side are performed across different length scales. The fissure-type porous-medium parameters are systematically varied in the porosity range $0.2 \leq \phi \leq 0.95$ and flow direction permeability $10^{-6} < K, m^2 < 10^{-9}$. From the exit-velocity profile, the empirical slip coefficient α is determined using a generalized relationship. When the measurements across the PM-CF interface are performed across a length scale equal to the representative elemental length (REL) of the porous media considered (i.e., equal to the sum of plate thickness (a) and gap (b)), the determined α value is found to remain invariant. [DOI: 10.1115/1.4026194]

Keywords: porous media, interface slip coefficient, PIV, hydraulic experiments, porous-medium experiments, numerical simulations, Beavers–Joseph interface condition

1 Introduction

Channel flow with partially filled porous-medium configuration is applicable in compact heat exchangers, electronic cooling, fuel cells, thermal insulation, oil recovery, and near-compact heat exchangers. In modeling such a configuration for studying transport of conservation quantities, a priori knowledge of the slip coefficient value at the interface between the porous-medium and clear-fluid flow is essential for closure.

By definition [1,2], a porous medium is a region of stationary solid matrix with interconnected pores sustaining a flow. A stack of parallel plates (schematic given in Fig. 1) with gaps encountering laminar flow fits this definition and is considered as porous media in this study. The test section shown in Fig. 1 also has a clear-fluid flow region above the porous region, making it a partially filled porous-medium channel flow.

Considering unidirectional flow, the momentum balance statement for the porous-medium flow is given by the differential form of the Darcy law as

$$\frac{dp}{dx} = -\frac{\mu}{K} u_D \qquad (1)$$

where dP/dx, N/m^3 is the applied pressure gradient, K, m^2 is the permeability of the porous medium, μ is the dynamic viscosity of the fluid, and u_D is the seepage speed or the cross section–averaged Darcy velocity. On the clear-fluid flow region (without porous medium) of Fig. 1, the steady-state momentum balance in the x direction is given by the Navier–Stokes equation

$$\rho(\nabla . u_f) u_f = -\nabla p + \mu \nabla^2 u_f \qquad (2)$$

The interface is subjected to normal and tangential stresses of different origins and magnitudes at the top and bottom planes. Beavers and Joseph [3] provided an interface boundary condition through the empirical relationship

$$\frac{\partial u}{\partial y}\big|_{y^+} = \alpha \frac{u_f - u_D}{\sqrt{K}} \qquad (3)$$

where u_f is the velocity in the clear-fluid flow region and u_D is Darcy or seepage velocity in the porous medium. The quantity α is an interface slip coefficient, and Eq. (3), in principle, is the constitutive equation that defines this quantity.

To determine α, the other quantities must be measured using experiments. It is understood from Refs. [2] and [3] that u_f and $\partial u_f / \partial y$ are evaluated at $y = 0^+$ and u_D is evaluated at some small distance from the $y = 0$ plane. The arbitrariness of the locations for measuring the quantities involved in Eq. (3) has been a topic of research interest and remains to be resolved. By looking at the form of Eq. (3), one could conjecture that the $\partial u_f / \partial y$, u_f in the clear-fluid region and the u_D on the porous-medium region are to be measured at points separated by a distance not less than $\sqrt{K}$, their gradient length scale.

The simplest way to arrange these points is to bisect the $\sqrt{K}$ length scale by the interface. Beavers and Joseph [3] first measured α using the above procedure for different porous media. A linear dependence of α on the porosity was observed. Experimental and analytical determination of α are reported by Taylor [4] and Richardson [5], where the porous medium consists of vertically grooved plates (similar to Fig. 1, but the plates are arranged vertically), over which a moving parallel plate provides Couette flow.

Some observations on the above equation are worth recalling. As proposed by Beavers and Joseph in Ref. [3], the constitutive
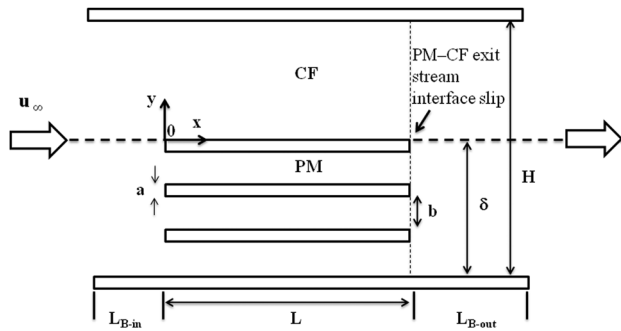
Fig. 1 2D schematic of partially filled porous-medium channel: The stacks of parallel plates (plate thickness *a* separated by uniform gaps *b*) treated as porous media extend until δ in y direction

1: Compressor, 2: Air dryer, 3: Pressure regulator, 4: Inlet valve, 5: Rotameter, 6: Seeder, 7: Settling Chamber, 8: Nd-Yag Laser, 9: Laser head, 10: optical arrangements, 11: Mirror, 12: CCD Camera, 13: Test section

Fig. 2 Schematic of the experimental setup
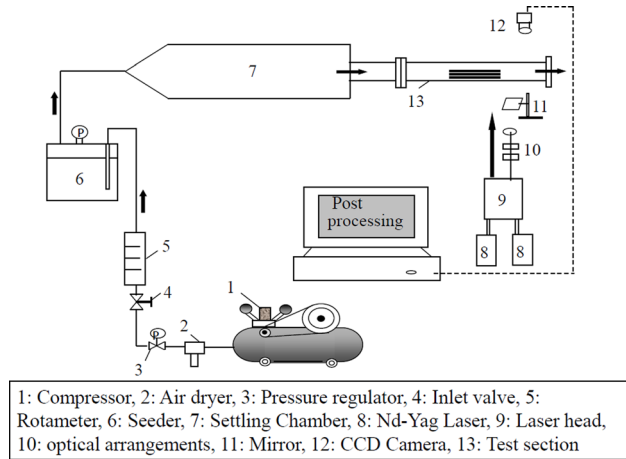
equation for the interface slip coefficient α is empirical in origin. From the original paper of Beavers and Joseph [3] and from the recent summary of interface results in Ref. [2], one can understand that, in Eq. (3), the y^+ at which the $\partial u_f/\partial y$ and u_f must be measured in the CF side is arbitrary. Similarly, y^-, the small distance from $y = 0$ at which u_D is measured in the PM side, is also arbitrary.

Additionally, it is a conjecture that the velocity profile $u(y)$ would vary continuously within a small distance across the interface between the CF and PM sides (see Fig. 1) and this small distance should be of $O(\sqrt{K})$. This remains to be established, with recent experimental evidence provided in Refs. [6] and [7] for a partially filled PM-CF configuration, suggesting the depth of penetration of flow in the porous medium is more than the $O(\sqrt{K})$.

The theoretical analysis presented by Vafai and Thyagaraja [8] shows that the analytical results of slip coefficient increase with decrease in the permeability, an opposite trend of their corresponding experimental data. Ochoa-Tapia and Whitaker [9] presented theoretical investigation of the interface boundary condition matching the Navier–Stokes equation and the Darcy equation for momentum balance. They reported a jump in the shear stress but not in the velocity, with the stress jump being inversely proportional to the permeability of the porous medium. These results were later used by Kuznetsov in Refs. [10] and [11] to provide analytical solutions for the flow field near the interface region, accounting for the boundary and inertial effects. The status of theoretical interface models was reviewed in Ref. [12]. The slip coefficient resulting from the above approach is yet to be systematically validated using experiments for all kinds of porous media. Gupte and Advani [13] performed local-density approximation experiments to determine the flow field near the permeable boundary of a porous medium. The boundary-layer thickness across the interface between the porous-medium and the clear-fluid flow was found not to be $O(\sqrt{K})$.

Sahraoui and Kaviany [14] found in their experiments that the determined slip coefficient could depend on the Reynolds number governing the overall flow. Further, recent experiments using PIV were reported by Shams et al. in Ref. [15] for the interface flow field between an annular array of cylinders forming the porous medium adjacent to Couette flow region and in Ref. [16] for shear flow penetrating a porous medium made of a regular array of rods of different cross sections. Both these experiments, while providing data of flow near the interface, did not investigate the appropriateness of the length scales in Eq. (3) for determining the slip coefficient. Goharzadeh and Jorgensen [6], through their experiments, suggested that the transition region across such an interface is of the order of the grain diameter, much larger than the $\sqrt{K}$ length scale.

Agelinchaab and Ruth [7] using PIV experiments measured the velocity of flow through circular cylindrical rods installed vertically in a channel. They measured the slip velocity at the interface between the rods and the clear-fluid flow, showing that the measured slip velocity depends only on the filling fraction. They reported that the depth of the open flow into the porous medium is more than $\sqrt{K}$. From the above experimental observations, it is evident that there is no clear justification for choosing $\sqrt{K}$ as the length scale across which the variables must be measured. Even at the differential level, Eq. (1) is defined and valid only in a solid-fluid volume-averaged porous continuum scale [17]. This scale is definitely larger than the scale of the fluid continuum in which Eq. (2) is defined. An interface boundary condition, such as Eq. (3), should consistently connect both the scales.

This paper presents results from extensive PIV experiments and numerical simulations performed for the configuration in Fig. 1, with the stack of parallel plates modeled as a standard fissure-type porous medium (page 350 of Ref. [18]) experiencing Darcy flow [19]. The objective is to determine the interface slip coefficient α using Eq. (3) with suitable modifications, with due attention to the continuum and porous continuum length scale validity of Eqs. (1) and (2).

2 Experimental Setup and Procedure

Figure 2 shows the schematic of the PIV experimental apparatus used to measure the flow field for the configuration shown in Fig. 1. The experiments are performed at an inlet average velocity of $U = 15$ cm/s, which corresponds to a Re = 388. The test section is 300 mm long and of rectangular cross section having a height of 30 mm and width of 60 mm (see Fig. 1). To aid undiffracted laser passage through the test section, all sides of the test section are made of glass.

Stacks of transparent parallel plates are considered as a porous medium in this study. They are constructed by mounting a stack of plates of $L = 108$ mm, width $w = 60$ mm, and thickness $a = 0.5 - 4$ mm at the bottom of the test section, as shown in Fig. 1. Table 1 provides the geometry and arrangement of several configurations of stacks of parallel plates, modeled as porous medium. The porosity range of $0.2 \leq \phi \leq 0.95$ is achieved by using different plate thickness (0.5 mm $\leq a \leq 4$ mm) and spacing (1 mm $\leq b \leq 7$ mm) between the plates. For a given plate thickness and the spacing between the plates, the permeability of the stack of plates can be determined [18] by using the relation $K = b^3/12(a+b), \text{m}^2$, resulting in a corresponding permeability range of $10^{-6} < K, \text{m}^2 < 10^{-9}$ for the models tested in this study. These models are arranged inside the test section such that they fill half the height, $\delta = h/H = 0.5$, to form a channel partially filled by an anisotropic fissure-type porous medium. This configuration enables one to rigorously characterize the slip coefficient between the fluid streams exiting the porous-medium and clear fluid section (see Fig. 1) as a function of the porous-medium

Table 1   Parameters of the porous-medium models. (All are assembled inside the test section, shown in Figure 1, with $\delta = H/2$.)

Model No.	Plate thickness (a, mm)	Pore diameter (b, mm)	No. of plates n	Porosity ϕ	K m^2	$\sqrt{K}$ mm mm	REL $= a + b$ mm
1	0.15	2.35	6	0.94	4.35×10^{-7}	0.65	2.5
2	0.5	2	6	0.8	2.67×10^{-7}	0.51	2.5
3	1	1.5	6	0.6	1.12×10^{-7}	0.3	2.5
4	2	0.5	6	0.2	4.17×10^{-9}	0.06	2.5
5	1	4	3	0.8	1.067×10^{-6}	1	5
6	2	3	3	0.6	4.5×10^{-7}	0.6	5
7	2.5	2.5	3	0.5	2.6×10^{-7}	0.5	5
8	3	2	3	0.4	1.33×10^{-7}	0.3	5
9	4	1	3	0.2	1.66×10^{-8}	0.1	5
10	0.5	7	2	0.93	3.8×10^{-6}	1.95	7.5
11	1	6.5	2	0.86	3.05×10^{-6}	1.75	7.5
12	2	5.5	2	0.73	1.84×10^{-6}	1.35	7.5
13	4	3.5	2	0.46	4.7×10^{-7}	0.69	7.5
14	5	2.5	2	0.33	1.74×10^{-7}	0.41	7.5
15	6	1.5	2	0.20	3.75×10^{-8}	0.19	7.5

properties. For the channel cross section length-scale–based Re = 388, the flow inside the stack of plates is verified to have a plate-gap–based Re value less than 0.1. It has been established (see Refs. [17], [20], and [21]) that, for these Re $\leq$ 0.1 values, the flow through fissure-type porous medium can be modeled as Darcy flow (Eq. (1)).

To perform PIV, the air flow in the test section is seeded with monodisperse oil droplets of $2\,\mu$m size. A double-pulsed Nd-YAG ($\lambda = 532$ nm) with an energy of 50 mJ per pulse is used in this study. The laser beam is converted into a light sheet using a combination of cylindrical lenses. This laser sheet is steered to pass through the $z = 0$ plane. A high-resolution (1208×1124), interline-transfer, digital charge-coupled device (CCD) camera (Pixelfly make of PCO Imaging, Germany) is used to image the flow field in the PIV.

Several PIV realizations of the steady laminar flow field are obtained in each experimental run, with the field view of the CCD camera chosen as 45×40, and more than 100 images are captured. The velocity field is determined as an average of these realizations. The PIV raw images are processed using PIVVIEW software (PIVTEC make), with a multigrid algorithm to extract a wide range of velocities. The final window size is 32×32 pixels with a 50% overlap. An uncertainty of $\pm 1\%$ is estimated in the instantaneous velocity, based on the characteristic displacement of eight pixels (as detailed in p. 164 of Ref. [22]). The velocity field is determined as an average of several PIV realizations.

3   Numerical Methods and Boundary Conditions

The schematic in Fig. 1 shows the computational domain and coordinate system of the partially filled stack of parallel plates in a rectangular channel. Steady and laminar incompressible flow is assumed in the direct simulation of the arrangement. The usage "direct simulation" should not be confused with Direct Numerical Simulation (DNS)-type simulation of turbulent flows. By "direct," it is meant that the porous-medium geometry is directly considered, instead of the "volume averaging methods" that are conventionally employed to study such flows (pp. 3–4 of Ref. [2]). This direct treatment of flow through the pores—equivalent to what actually happens in the corresponding experiments explained earlier—enables the use of laminar flow simulations using the standard Navier–Stokes equations.

The governing equations of mass and momentum balance used in the simulations are

$$\nabla \cdot \vec{u} = 0 \tag{4}$$

$$\rho(\nabla \cdot \vec{u})\,\vec{u} = -\nabla p + \mu \nabla^2 \vec{u} \tag{5}$$

The above conservation equations are solved in the domain of Fig. 1 for each PM-CF model configuration given in Table 1. At the plate walls, no-slip boundary condition is imposed and both components of velocity. An outflow condition ($\partial u / \partial x = 0$, $v = 0$) is imposed at the exit. The numerical simulations were performed in 2D at the midplane ($z/2$) of the test section domain in Fig. 1. This is then compared with the experimental results obtained at the identical midplane using the setup discussed earlier.

The flow upstream to the test section inlet is set to a known uniform velocity field $u(y) = U$. Sufficient buffer length L_{B-in} is provided between the inlet boundary and the test-section inlet to allow flow similar to that in the experiment. Similarly, fully developed flow condition is imposed at a distance L_{B-out} downstream of the test section exit $x = L$. All these boundary conditions are given in nondimensional form in Fig. 1.

These governing equations are discretized using the finite volume method, and the resulting equations are solved in an iterative procedure using the standard implicit, second-order upwind solver with the velocity and pressure coupling achieved by the SIMPLE algorithm [23]. The convergence criterion for the continuity and momentum equation residuals are set as 10^{-3} and 10^{-6}, respectively. The grid independence test based on the exit velocity profile is conducted for four successive grid levels. Quadrilateral uniform grid in both x and y directions are used to cover the computational domain. The exit velocity profile is calculated for four successive grid levels (20×249, 40×499, 80×996, and 160×1992) at the maximum Re = 388 of the conducted experiments (Re based on hydraulic diameter $= \rho U D_h / \mu$) for flow through the stack of parallel-plate channel. The errors in the exit velocity profile and the total pressure drop across the test section between two successive levels of grid refinement are checked to be less than one percent. Based on this, a quadrilateral uniform grid in both x and y directions with 80×996 grid points in the fluid zone with 79,716 nodes is chosen and used over the computational domain of Fig. 1.

As a validation of the experimental setup and the numerical simulation procedure, Fig. 3 shows the comparison of $u(y)$ at midplane at z direction, at the exit of the channel without the porous medium. The unfilled squares and filled triangles mark data obtained from the present experimental and numerical study, respectively, for Model-10 (see Table 1). They are compared with the analytical solution for fully developed flow between parallel plates from White [24]. The slight reduction in the maximum velocity measured in the experiment is possibly due to the rectangular bounding-channel side wall effect, which is absent in the analytical solution for the parallel plates. Nevertheless, the comparison shows good agreement with the maximum error <5% between the experiment and analytical results.
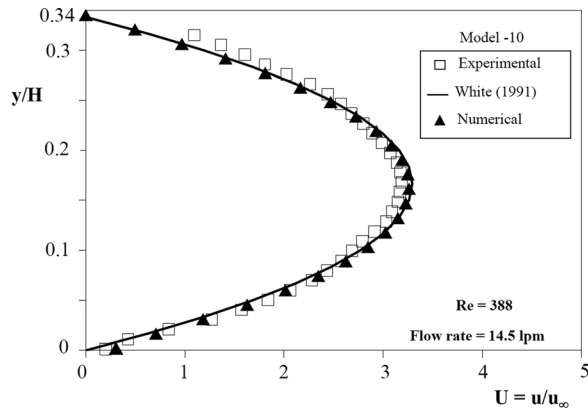
Fig. 3 Comparison of present experimental data with theory [24]

4 Results and Discussion

Figures 4(a)–4(d) show velocity vectors from experiments and numerical simulations, inside the stack of parallel plates for Model-6 ($\phi = 0.6$), and Model-8 ($\phi = 0.4$). The velocity vector fields are obtained in the experiments over a domain of 45×15 mm bounded by 10 mm upstream from exit and 15 mm from the axis. Comparing Figs. 4(a) and 4(b), the velocity vectors inside the stack of plates obtained from both experimental and numerical data are seen to match well for the entire flow field. Similarly, the velocity vector fields for Model-8 in Figs. 4(c) and 4(d) show good agreement. The magnitude of velocity increases with increase in the solid volume fraction $(1 - \phi)$ of the porous medium.

Figures 5(a) and 5(b) show data for the local velocity profiles obtained from the PIV measurement near the exit of the test section for Model-6 and Model-8. The continuous curves in Fig. 5 indicate the corresponding results obtained using direct numerical simulation of the configurations. In response to a reviewer query, it should be mentioned that the results from these models are discussed here only as an indicative sample. Flow through the test
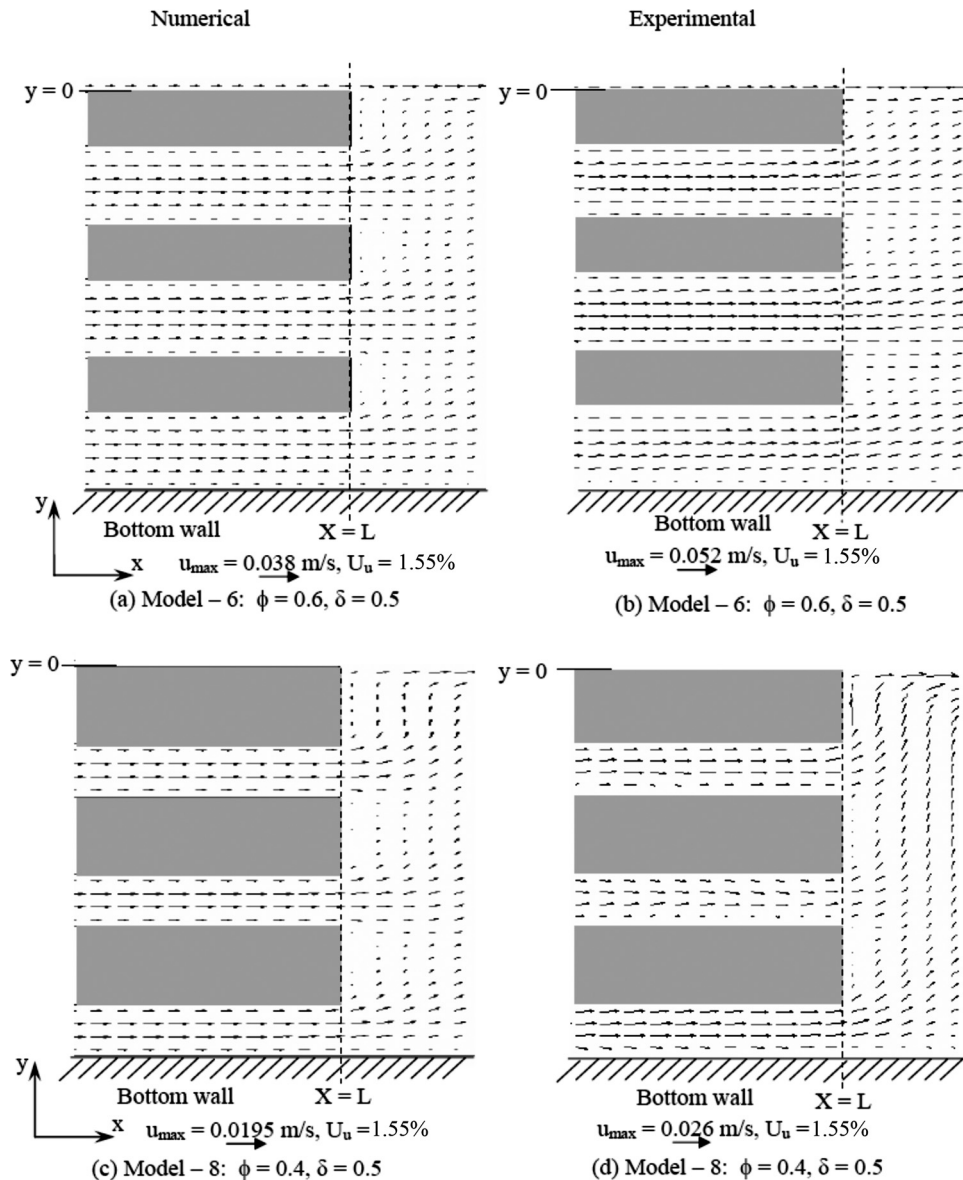
Fig. 4 Velocity vectors at the exit PM-CF slip-interface for various void fractions
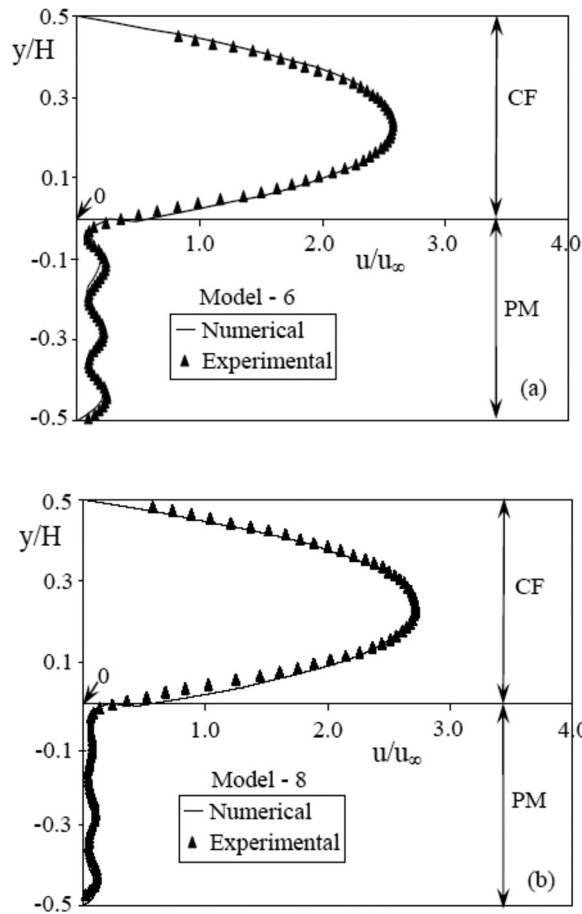
Fig. 5 Comparison of PIV experimental exit-velocity profile data with corresponding numerical simulations for (a) Model-6 and (b) Model-8

Fig. 6 Exit velocities averaged over several channel heights in the porous-medium region

section for the rest of the models listed in Table 1 also exhibit similar behavior and are subjected to subsequent analysis.

The velocity data is always nonzero along the y direction, contrary to the expected intermittent zero values at the plates, because the plot is obtained at a location 3 mm downstream from where the stack of plates end ($x = L$). The good agreement between the data from experiments taken at midplane in the z direction and the results from the two-dimensional numerical simulations corroborate the prevailing two-dimensional flow in the configuration.

Observe, in the PM zone of Fig. 5(a), the parabolic velocity profile at the bottom-most pore level is consistently of higher magnitude compared to the rest of the corresponding pore velocity profiles, although only marginally. This is because of the presence of a recirculation zone behind the stack of parallel plates formed due to the higher average velocity of the top CF region with respect to the PM region flow. Evidence of this recirculation zone is observed in both experiments and simulations, as shown in the velocity profiles of Figs. 4(a) and 4(b). Comparing Figs. 5(a) and 5(b), for a fixed $(a + b)$, as the solid volume fraction $(1 − \phi)$ increases, the pore level flow reduces, diminishing the recirculation effect.

Volume averaging the porous-medium flow region is a basic notion for formulating the momentum equations for porous-medium flows over a porous continuum [1,25]. In a general three-dimensional porous continuum, each point is equivalent to a representative elemental volume (REV) of the porous medium. The REV can be defined as the smallest length scale at which any considered porous-medium property (in this case, the u_D) becomes invariant to locations of determination (p. 3 of Ref. [2]). Obviously, Eq. (1) is defined over such a porous continuum, with
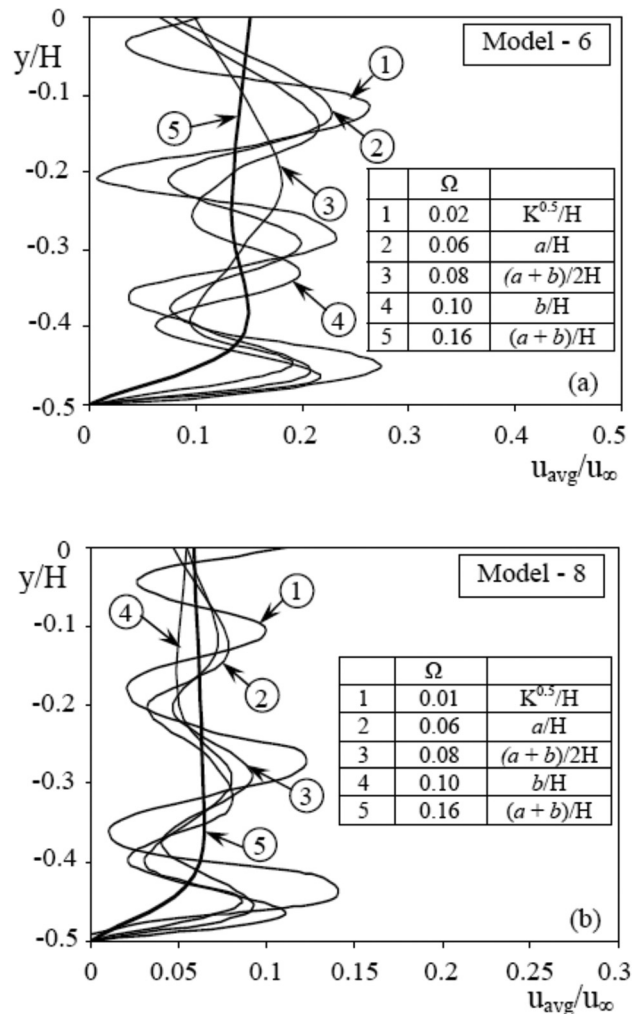
points equivalent to a finite REV. Further, for the stack of parallel plates shown in Fig. 1, considered as homogeneous fissure-type porous medium, the representative elemental volume (REV) can vary only in the y direction. This results in the REV essentially becoming a representative elemental length (REL) for these porous media.

Taking the Darcy velocity u_D, of Eq. (1) as a property to determine the REL for the considered porous media, its invariance across the y direction length variation can be checked. The correct REL is that smallest length scale (in y direction in this porous media) at which u_D remains invariant. This procedure is shown in the results of Fig. 6 and in the following discussion.

Figure 6 shows the results of averaging $u(y)$, the experimentally determined local velocities of Fig. 5, over several progressively increasing length scales to determine an invariant u_D, the Darcy velocity. For instance, in Fig. 6(a), the curve marked 1 is obtained by joining the representative values of u_D found by averaging $u(y)$ measured at successive locations separated by $y^+ = \sqrt{K}$ in the PM zone. The locus at the bottom wall is taken as $u_D = 0$ to satisfy no-slip condition. The rest of the curves, from 2 to 5, are obtained following a similar averaging procedure over other possible candidate length scales for the REL, when the stack of plates is treated as a porous medium.

The curve marked 5 results in an invariant u_D yielding a REL $= (a + b)$ for this porous configuration. Hence, for such a stack of plates considered as porous medium, the REL is equal to $(a + b)$, as at that spatial resolution, u_D becomes invariant to
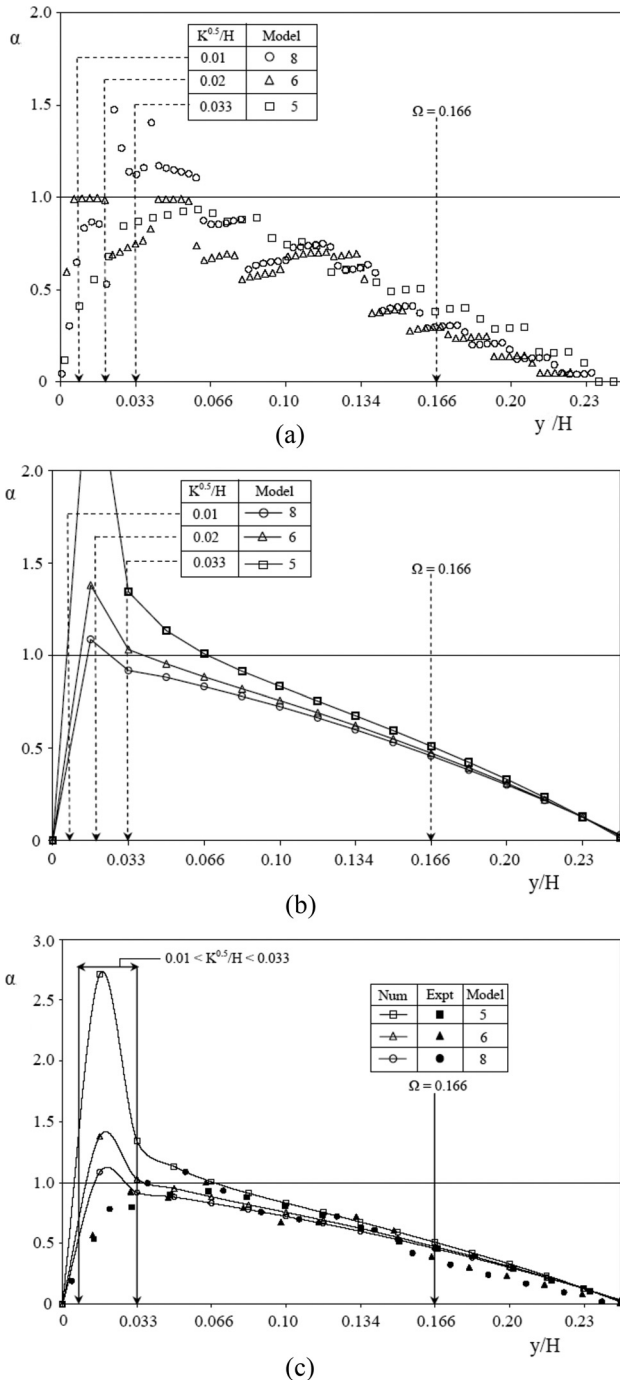
Fig. 7 α versus y/H for REL, $\Omega = 0.166$ models: (a) PIV experiments, (b) numerical simulation, and (c) combined results

locational determination. Likewise, for Model-8, the REL can be deduced to be equal to $(a + b)$ from the determination of u_D shown in Fig. 6(b). For both Model-6 and Model-8, the RELs are identical and equal to 5 mm. Results from the corresponding numerical simulations also yield identical values of REL for these models. The RELs for all of the models tested in experiments and simulations are given in the last column of Table 1.

Having determined the u_D and the associated REL, one can proceed to determine the interface slip coefficient α using the empirical relation proposed in Ref. [3] in the form

$$\alpha_{B-J} = \frac{(\partial u_f / \partial y)|_{y^+}}{u_f - u_D/\sqrt{K}} \qquad (6)$$

which is a modified representation of Eq. (3). Hence, the arbitrariness of the length scales involved, as discussed in Sec. 1 hold.

Attempts have also been made in the past, in particular by Saffman [26], to provide a theoretical foundation for the slip coefficient as originating from the stress jump across the interface due to mismatch of longitudinal momentum. But following the original suggestion in Ref. [3] and treating the slip coefficient as an empirical relationship to maintain the velocity continuity at the interface, one requires only to remove the arbitrariness of the spatial locations where the measurements need to be made to obtain, if possible, a unique α for a PM-CF configuration.

Embarking on such a procedure, to find a slip coefficient that serves the purpose of the empirical nature of α, we generalize and rewrite Eq. (6) as

$$\alpha = \frac{(\partial u_f / \partial y)|_{y^+}}{u_f - u_D/(2y^+)} \qquad (7)$$

Observe in Eq. (7) the use of y^+ instead of the $\sqrt{K}$ used in Eq. (6). In Eq. (7), the parameters u_f and $\partial u_f / \partial y$ must be measured at a distance y^+ away from the interface and the u_D must be measured at y^- on the PM side.

One can now try to find suitable values for y^+ and y^-, where the quantities involved in Eq. (7) need to be measured. Taking $y^+ = y^-$ for simplicity, it could be argued that the pore diameter (b), the particle diameter (a), or the permeability (K) of the porous medium are all possible candidates for being the y^-, depending on the extent of penetration of the external (clear-fluid) flow through the interface and into the porous medium.

To arrive at a possible fixed value of y^+ for the porous medium modeled in this study, we follow this reasoning: Since the u_D is the Darcy velocity or the seepage speed, it must be measured at or above the representative elemental volume (REV) of the porous medium considered. In the present case, as explained earlier, the REV is only an REL. Importantly, this observation implies irrespective of the distance from the interface at which the measurement is done in the porous medium (i.e., the y^- measurement); the Darcy velocity measurement is valid only in the REL-averaged porous continuum scale. Such a measurement is possible only across multiples of RELs. This physical restriction of the momentum balance model in the porous medium rules out the interpretation that the y^- in the porous medium could be equal to the pore diameter, particle diameter, or the permeability of a porous medium. The actual measurement of velocities in the porous-medium side at such length scales could result only in the local (pore-scale) velocity, not u_D, the Darcy velocity that one should measure according to Eq. (7).

Based on the above discussion, it can be conjectured that $y^+ = y^- = \text{REL} = (a + b)$ for the stack of parallel plates considered as porous medium here. To test this hypothesis, α is determined using Eq. (7) using the experimental $u(y)$ data for three models of REL $= 5$ mm (see Table 1). The u_D valid over a REL can be determined from the averaging procedure explained in Fig. 6 (for Model-6 and Model-8). For each model, the other necessary quantities u_f and $\partial u_f / \partial y$ are measured at several y^+ locations, including the probable and suitable length scales discussed earlier.

Figure 7 plots the variation of α with y for the above models. The α values determined from the PIV data for the three models are given in Fig. 7(a). Figure 7(b) shows the corresponding α values determined from numerical simulation for the three models under identical flow conditions. Since the step size in y in the experiment is smaller than the grid size in the numerical simulations, the experimental data is suitably averaged and the corresponding α values are replotted in Fig. 7(c) along with those determined from the simulations.

The immediate observation from Figs. 7(a) to 7(c) is that the value of α, if determined at a length scale comparable to $\sqrt{K}$ is very different for each of the models, even though they all are of
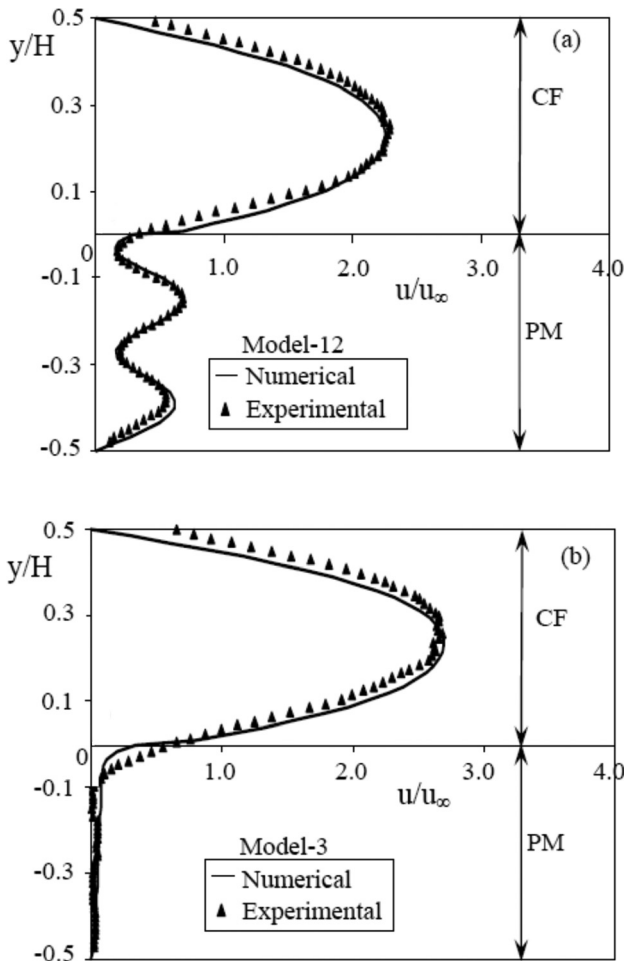
Fig. 8 Velocity vectors for (*a*) Model-12 with REL = 7.5 mm and (*b*) Model-3 with REL = 2.5

identical REL (= 5 mm). On the other hand, the α value determined at REL = 5 mm has very little scatter. This observation is true for all the three models and for both experimental and numerical results, as seen in Fig. 7(*c*).

This suggests that $\sqrt{K}$ length scale is not necessarily the correct length scale to measure the velocities and their gradients for determining α, the slip coefficient. It further supports that the REL of the porous medium could be an alternative length scale.

This conjecture is further tested with porous-medium models grouped into two other REL values, namely, REL = 7.5 mm and REL = 2.5 mm, as listed in Table 1. Figures 8(*a*) and 8(*b*) show, for $Re = 388$, the exit $u(y)$ for Model-12 (REL = 7.5 mm) and Model-3 (REL = 2.5 mm) obtained from experiments and corresponding numerical simulations. In both the figures, the $u(y)$ obtained from numerical simulations predicts the experimental velocity profile within 5%.

For all these models, the determined α values are shown in Fig. 9(*a*) with respect to y/H, as before. Numerical simulations are performed for all the 15 models given in Table 1. Figure 9(*b*) plots the α values determined from these results. Figure 9(*c*) merges the α values obtained from experiment and numerical simulations through a suitable averaging of the experimental data, as explained before for Fig. 7(*c*).

The three REL values (expressed nondimensionally as Ω) tested in this study are marked along the abscissa of Figs. 9(*a*)–9(*c*). Also given is the range of $\sqrt{K}$ values for the models. It is evident from Fig. 9(*c*) that, for all the models tested in this study, the range of $\sqrt{K}$ is about one order less than the corresponding REL
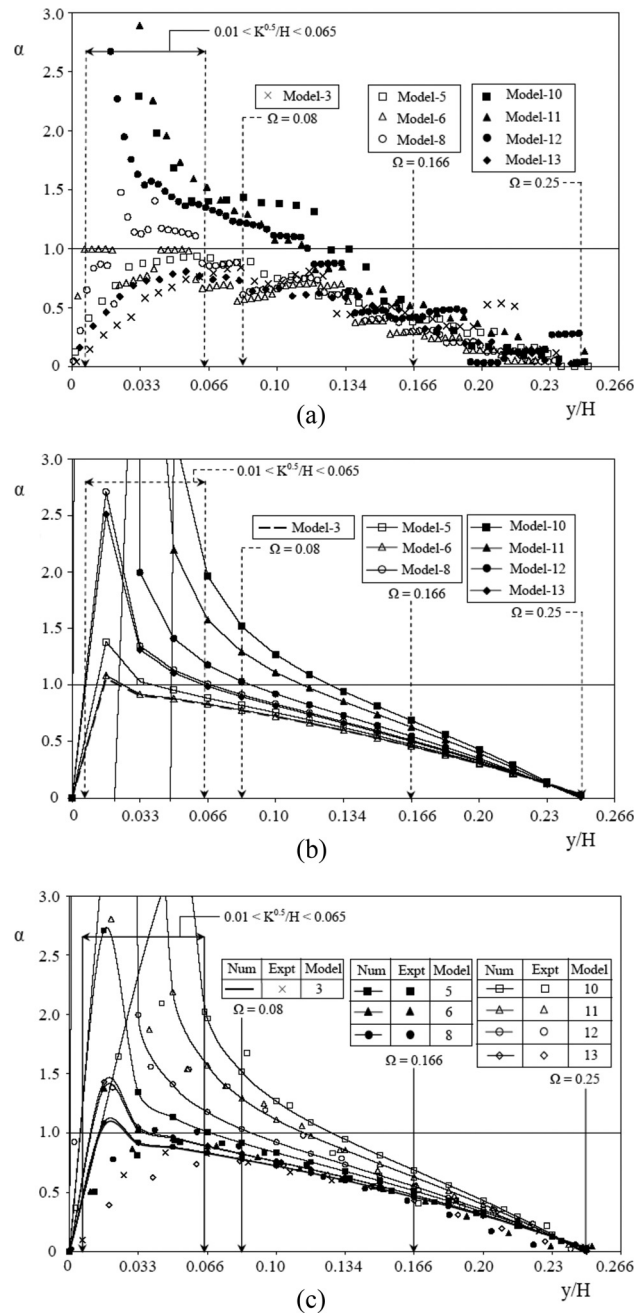

Fig. 9 α versus y/H for all 15 models in Table 1 (comprising three REL values): (*a*) PIV experiments, (*b*) numerical simulation, and (*c*) combined results

values. The α values determined using quantities measured across a length scale of $\sqrt{K}$ show large scatter when compared with that determined using parameters measured at the REL length scale across the interface.

Figure 10 shows the α values determined from Eq. (7) using quantities determined at locations across the interface separated by a distance equal to the $\sqrt{K}$ of each PM-CF configuration considered. Similarly, Fig. 11 shows the α values determined from Eq. (7) using quantities determined at locations across the interface separated by a distance equal to the REL of each PM-CF configuration considered.

From Fig. 11, it is evident that the α value thus determined increases when the REL of the porous-medium configuration decreases. As the REL decreases, the permeability K of the porous medium also decreases, resulting in less flow through the porous
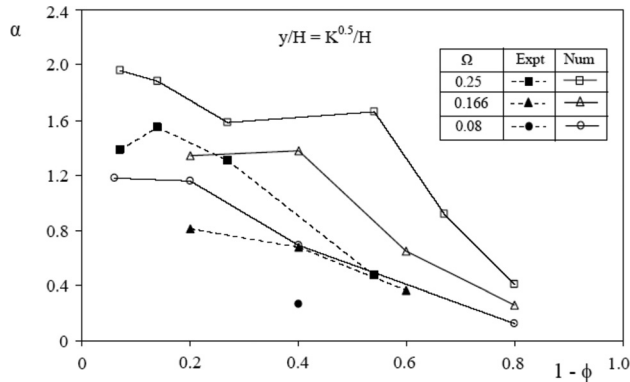
Fig. 10 Interface slip coefficient α variation with solid volume fraction. Parameters determined at $\sqrt{K}$ distance across the interface.
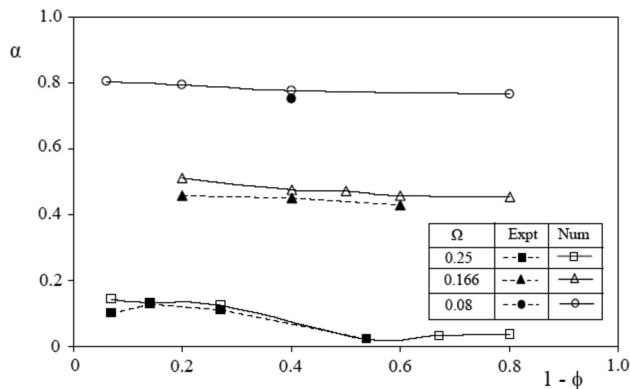
Fig. 11 Interface slip coefficient α variation with solid volume fraction. Parameters determined at REL distance across the interface.

medium. As the overall flow rate remains fixed, this leads to increased flow on the clear-fluid side, above the interface. This results in a larger velocity gradient across the interface, leading to higher values of α as the REL decreases. It is worth recalling that no such reasoning is possible with the data presented in Fig. 10, where the α value is determined using parameters measured across a distance of $\sqrt{K}$ over the interface.

Further, it is also evident from Fig. 11 that, for a REL, the α value remains invariant (almost a constant) to porosity variation for the range of solid volume fraction $0.6 < 1 - \phi < 0.8$. This interesting result, corroborated by the experiments and corresponding simulations, allows one to conjecture the REL of a porous medium as the possible length scale across which the u_D, u_f, and $\partial u_f / \partial y$ are to be measured for determining the slip coefficient α. The REL length scale of a porous medium is usually larger than the $\sqrt{K}$ length scale proposed in Ref. [3]. Further experiments with other type of porous media are required to establish this conclusion.

5 Conclusions

From measurements performed using PIV experiments and direct numerical simulations, the interface slip coefficient, designated α, is determined at the slip interface between clear-fluid and porous-medium flow streams exiting a partially filled porous-medium channel. Stacks of parallel plates placed horizontally inside the channel were the standard fissure-type anisotropic porous-medium configuration considered in order to simplify the

occurrence of slip only at the exit. The plate thickness and gaps were varied to provide three different representative elemental length (REL) for the porous medium, with porosity varying in the range $0.2 \leq \phi \leq 0.95$, yielding a wide permeability range of $10^{-6} < K, \mathrm{m}^2 < 10^{-9}$. For a fixed cross section–averaged Re = 388, the interface slip coefficient α was determined using local velocity measurements at the exit section of the porous medium.

The major conclusions from the results are:

For all the parallel-plate fissure-type porous-medium models tested in this study, the α, determined at the exit using parameters measured across a length-scale of $\sqrt{K}$ show large scatter.

When it is determined using quantities measured across the interface at a length scale of the REL of the porous medium, the α values showed little scatter and remained almost a constant. For a REL, the α value remains invariant in the test range of porosity $0.2 \leq \phi \leq 0.95$.

By using the REL of the porous medium as the length scale, the prevailing arbitrariness appears removed. This conclusion is corroborated by both the PIV experiments and corresponding simulations.

For the simple fissure-type porous-medium models (stack of parallel plates), the REL length scale is about one order larger than their $\sqrt{K}$, the conventional length scale suggested for α determination.

Further experiments with other types of porous media, allowing a developing interface cross flow, are required to establish the generality of these conclusions.

References

[1] Whitaker, S., 1999, *The Method of Volume Averaging*, Kluwer Academic, The Netherlands.
[2] Nield, D. A., and Bejan, A., 2006, *Convection in Porous Media*, Springer, New York.
[3] Beavers, G. S., and Joseph, D. D., 1967, "Boundary Conditions at a Naturally Permeable Wall," J. Fluid Mech., **30**, pp. 197–207.
[4] Taylor, G. I., 1971, "A Model for the Boundary Condition of a Porous Material. Part 1," J. Fluid Mech., **49**, pp. 319–326.
[5] Richardson, S., 1971, "A Model for Boundary Condition of a Porous Material. Part 2," J. Fluid Mech., **49**, pp. 327–336.
[6] Goharzadeh, A., Khalili, A., and Jorgensen, B. B., 2005, "Transition Layer Thickness at a Fluid-Porous Interface," Phys. Fluids, **17**, p. 057102.
[7] Agelinchaab, M., Tachie, M. F., and Ruth, D. W., 2006, "Velocity Measurements of Flow Through a Model Three-Dimensional Porous Medium," Phys. Fluids, **18**, p. 017105.
[8] Vafai, K., and Thiyagaraja, R., 1987, "Analysis of the Flow and Heat Transfer at the Interface Region of a Porous Medium," Int. J. Heat Mass Transfer, **30**, p. 1391.
[9] Ochoa-Tapia, J. A., and Whitaker, S., 1995, "Momentum Transfer at the Boundary Between a Porous Medium and a Homogeneous Fluid-II Comparison With Experiments," Int. J. Heat Mass Transfer, **38**, pp. 2635–2646.
[10] Kuznestov, A. V., 1997, "Influence of the Stress Jump Condition at the Porous-Medium/Clear-Fluid Interface on a Flow at a Porous Wall," Int. Commun. Heat Mass Transfer, **24**, pp. 401–410.
[11] Kuznestov, A. V., 2000, "Analytical Studies of Forced Convection in Partly Porous Configuration," *Handbook of Porous Media*, K. Vafai, ed., Marcel Dekker, New York, pp. 269–312.
[12] Alazmi, B., and Vafai, K., 2001, "Analysis of Fluid Flow and Heat Transfer Interfacial Conditions Between a Porous Medium and a Fluid Layer," Int. J. Heat Mass Transfer, **44**, pp. 1735–1749.
[13] Gupte, S. K., and Advani, S. G., 1997, "Flow Near the Permeable Boundary of a Porous Medium: An Experimental Investigation Using LDA," Exp. Fluids, **22**, pp. 408–422.
[14] Sahraoui, M., and Kaviany, M., 1992, "Slip and No-Slip Velocity Boundary Conditions at Interface of Porous Plain Media," Int. J. Heat Mass Transfer, **35**, pp. 927–943.
[15] Shams, M., Currie, I. G., and James, D. F., 2003, "The Flow Near the Edge of a Model Porous Medium," Exp. Fluids, **35**, pp. 193–198.
[16] Tachie, M. F., James, D. F., and Currie, I. G., 2003, "Velocity Measurements of Shear Flow Penetrating a Porous Medium," J. Fluid Mech., **493**, pp. 319–343.
[17] Lage, J. L., Krueger, P. S., and Narasimhan, A., 2005, "Protocol for Measuring Permeability and Form Coefficient of Porous Media," Phys. Fluids, **17**(8), p. 088101.
[18] Bejan, A., 1997, *Convection Heat Transfer*, Wiley, New York.
[19] Wilson, L., Narasimhan, A., and Venkateshan, S. P., 2006, "Permeability and Form Coefficient Measurement of Porous Inserts With Non-Darcy Model Using Non-plug Flow Experiments," ASME J. Fluids Eng., **128**, pp. 638–642.

[20] Papathanasioua, T. D., Markicevic, B., and Dendy, E. D., 2001, "A Computational Evaluation of the Ergun and Forchheimer Equations for Fibrous Porous Media," Phys. Fluids, **13**(10), pp. 2795–2804.

[21] Lage, J. L., and Antohe, B. V., 2000, "Darcy's Experiments and the Deviation to Nonlinear Flow Regime," ASME J. Fluids Eng., **122**, pp. 619–625.

[22] Raffel, M., Willert, C., and Kompenhans, J., 1998, *Particle Image Velocimetry - A Practical Guide*, 2nd ed., Springer, Berlin.

[23] Patankar, S. V., 1980, *Numerical Heat Transfer and Fluid Flow*, Taylor and Francis, London.

[24] White, F. M., 1991, *Viscous Fluid Flow*, McGraw-Hill, New York.

[25] Narasimhan, A., 2012, *Essentials of Heat and Fluid Flow in Porous Media*, CRC, Boca Raton, FL.

[26] Saffman, P. G., 1971, "On the Boundary Condition at the Surface of a Porous Medium," Stud. Appl. Math., **1**, pp. 93–101.